Monthly Notices of the ROYAL ASTRONOMICAL SOCIETY

MNRAS **508,** 2848–2854 (2021) https://doi.org/10.1093/mnras/stab2655
Advance Access publication 2021 October 7

Temperature-dependent direct photodissociation cross sections and rates of AlCl

Zhi Qin [1,2] Tianrui Bai[1,3] and Linhua Liu [1,3,4]★

[1]*Optics and Thermal Radiation Research Center, Institute of Frontier and Interdisciplinary Science, Shandong University, Qingdao, Shandong 266237, China*
[2]*School of Information Science and Engineering, Shandong University, Qingdao 266237, China*
[3]*School of Energy and Power Engineering, Shandong University, Jinan 250061, China*
[4]*School of Energy Science and Engineering, Harbin Institute of Technology, Harbin 150001, China*

Accepted 2021 September 10. Received 2021 September 10; in original form 2021 August 15

ABSTRACT

The photodissociation process of aluminium monochloride (AlCl) plays an important role in modelling the chemistry of the circumstellar envelope. In this work, direct photodissociation cross sections of AlCl have been computed for transitions from the ground $X^1\Sigma^+$ state to six low-lying excited electronic states by using *ab initio* potential energy curves and transition dipole moments, which are obtained by the internally contracted multireference configuration-interaction method with Davidson correction and the aug-cc-pV6Z basis set. State-resolved cross sections for transitions from 38 958 rovibrational levels ($\upsilon'' \leq 100$, $J'' \leq 400$) of the ground $X^1\Sigma^+$ state have been obtained for photon wavelengths from 500 Å to the dissociation threshold. Photodissociation cross sections in local thermal equilibrium are evaluated for gas temperatures from 500 to 10 000 K. Using the computed cross sections, temperature-dependent photodissociation rates of AlCl in the interstellar and blackbody radiation fields are determined. The results can be applied to the investigation of the chemical evolution of Al in the envelope of carbon-rich and oxygen-rich stars.

Key words: astrochemistry – molecular data – molecular processes – ISM: molecules.

1. INTRODUCTION

Research on molecular photodissociation dates back to the 1920s and 1930s, when the importance of photodissociation was recognized in astrophysical applications (Eddington 1928; Kirby & Van Dishoeck 1989). Photodissociation can affect the abundances of atoms and small molecules in diffuse interstellar clouds (Kramers & Ter Haar 1946; Bates & Spitzer 1951; Black 1989; Kirby & Van Dishoeck 1989; Visser et al. 2009). Moreover, photodissociation can lead to the generation of many of the free radicals in cometary atmospheres (Crovisier et al. 1997; Benna et al. 2015; Bieler et al. 2015). More recently, the increasing realization of the critical role of photodissociation in modelling the gas-phase chemistry in various astrophysical media has caused great concern among astrophysicists (van Dishoeck 1998; van Dishoeck & Blake 1998; Lodders & Fegley 2006; Snow & Bierbaum 2008; Larsson et al. 2012; Grebenshchikov 2016; Valiev et al. 2020; Pezzella et al. 2021). All these applications can be attributed to the familiar fact that photodissociation is an important mechanism for the destruction of interstellar molecules in photon-dominated or photodissociation regions (PDRs).

Aluminium monochloride (AlCl) is a molecule of significant astrophysical interest and has been found in a variety of astrophysical objects. Some rotational lines at $\upsilon = 0$ for AlCl have been detected in the circumstellar envelope of the carbon-rich star IRC +10216 (Cernicharo & Guelin 1987; Agúndez et al. 2012). Agúndez et al. (2012) also evaluated the molecular abundance of AlCl in the inner circumstellar layers of IRC +10216 and reported an abundance relative to H_2 of 7×10^{-8}. AlCl has also been observed in oxygen-rich asymptotic giant branch (AGB) stars. Decin et al. (2017) detected AlCl in the dust formation region of the AGB stars, R Dor and IK Tau, in an attempt to identify Al-containing molecules by the Atacama Large Millimeter/sub-millimeter Array (ALMA) observations, and estimated a lower limit of atomic Al bearing in molecules. The fractional abundance structure [AlCl/H_2] was also established by Decin et al. (2017) using a non-local thermodynamic equilibrium (non-LTE) radiative transfer model of the circumstellar envelope (CSE). Moreover, Yousefi & Bernath (2018) predicted the possibility of detecting AlCl in the Sun's photosphere based on the estimated abundances of 1.73×10^{-6} and 3.16×10^{-7}, respectively, for Al and Cl relative to H (Asplund et al. 2009). In addition, Lodders & Fegley (2006) predicted the formation of AlCl in L- and T-type brown dwarfs below 2500 K.

For carbon-rich and oxygen-rich stars, interstellar ultraviolet photons can penetrate into the inner layers of CSEs and form PDRs, which may lead to photochemistry reactions of interstellar molecules. The photodissociation of AlCl is likely to occur by absorbing a photon

$$\mathrm{AlCl} + h\nu \rightarrow \mathrm{Al} + \mathrm{Cl}. \quad (1)$$

The resulting Al and Cl may participate in the formation of other molecules by radiative association, such as AlF, NaCl and KCl in the carbon-rich star IRC +10216 and AlO in oxygen-rich AGB stars. These molecular reactions, along with other chemical processes, can be used to create a chemical network that can evaluate the concen-

★ E-mail: liulinhua@sdu.edu.cn

trations of Al-bearing species in these astrophysical environments (Agúndez et al. 2012; Decin et al. 2017).

To the best of our knowledge, there is no previous work on the photodissociation of AlCl. The lack of photodissociation cross sections and rates of AlCl hinders the accurate estimation of its abundance. Here, we have computed the photodissociation cross sections of AlCl for several electronic transitions from a large range of rovibrational levels in the ground $X^1\Sigma^+$ state. The $2^1\Sigma^+ \leftarrow X^1\Sigma^+$, $A^1\Pi \leftarrow X^1\Sigma^+$, $2^1\Pi \leftarrow X^1\Sigma^+$, $3^1\Pi \leftarrow X^1\Sigma^+$, $4^1\Pi \leftarrow X^1\Sigma^+$ and $5^1\Pi \leftarrow X^1\Sigma^+$ electronic systems are considered. First, the state-of-the-art *ab initio* potential energy curves (PECs) and transition dipole moments (TDMs) are computed, as an input to obtain the state-resolved cross sections for the six electronic transitions mentioned above. Then, the state-resolved cross sections are applied to environments in LTE conditions where a Boltzmann distribution of initial rovibrational levels is assumed. Finally, temperature-dependent photodissociation rates of AlCl dissociated by the interstellar radiation field (ISRF) and the blackbody radiation field are produced.

The layout of this paper is as follows. A brief overview of *ab initio* electronic structure calculations of AlCl and the photodissociation theory is presented in Section 2. The computed PECs, TDMs, state-resolved photodissociation cross sections, LTE photodissociation cross sections and photodissociation rates of AlCl are discussed in Section 3, where we also compare the fitted spectroscopic constants and the computed TDMs with available theoretical and experimental results. Finally, we provide our conclusion in Section 4.

2. THEORY AND CALCULATIONS

2.1 *Ab initio* calculation

The electronic structure calculations were carried out with the MOLPRO 2015 quantum chemical package (Werner et al. 2015, 2020). The symmetry point group of AlCl is $C_{\infty v}$. Because MOLPRO cannot take advantage of the full symmetry of the non-Abelian group, all of the calculations were performed with the C_{2v} subgroup of the $C_{\infty v}$ point group. The corresponding relationship between the irreducible representations of both point groups is $\Sigma^+ \rightarrow A_1$, $\Pi \rightarrow B_1 + B_2$, $\Delta \rightarrow A_1 + A_2$ and $\Sigma^- \rightarrow A_2$. We computed 76 single point energies corresponding to the internuclear distances of 1.4−8.0 Å to obtain the PECs of the ground and six singlet excited states. The step length is 0.1 Å for R = 1.4−1.5 Å, 0.05 Å for R = 1.5−1.9 Å, 0.02 Å for R = 1.9−2.4 Å, 0.05 Å for R = 2.4−2.6 Å, 0.1 Å for R = 2.6−6 Å and 0.5 Å for R = 6−8 Å.

In our calculations, the augmented correlation consistent polarized sextuplet Gaussian basis set aug-cc-pV6Z (AV6Z) was used to describe the Al and Cl atoms. The specific calculation process is as follows. The single-configuration wavefunction of the ground X $^1\Sigma^+$ state of AlCl was generated by the Hartree–Fock calculations, and then it was optimized by the complete active space self-consistent field (CASSCF) method (Knowles & Werner 1985; Werner & Knowles 1985) to obtain the multiconfiguration wavefunction. In the CASSCF calculations, ten molecular orbitals (MOs) were put into the active space, including six a_1, two b_1 and two b_2, and these MOs correspond to the 3 *s* 3 *p* shell of the Al atom and 3 *s* 3 *p* shell of the Cl atom. The remaining electrons of the Al and Cl atoms were placed in closed orbitals. Finally, on the basis of the CASSCF wavefunctions, the dynamic correlation energies were computed by the internally contracted multireference configuration-interaction method including the Davidson correction (icMRCI + Q; Knowles & Werner 1988,1992; Werner & Knowles 1988; Shamasundar et al. 2011).

2.2 Photodissociation theory

The theory of the photodissociation cross sections has been detailed in many previous works (Weck et al. 2003; Loreau et al. 2011; Miyake et al. 2011; El-Qadi & Stancil 2013; Babb 2015; McMillan et al. 2016; Zammit et al. 2017; Pattillo et al. 2018; Xu et al. 2019; Yang et al. 2020; Bai et al. 2021; Qin et al. 2021). Here, we present a brief overview of this theory. In units of cm^{-1}, the expression of the state-resolved cross sections for a bound-free transition from the initial rovibrational level ($\upsilon''J''$) is given by

$$\sigma_{\upsilon''J''}(E_{\rm ph}) = 2.689 \times 10^{-18} \times E_{\rm ph} g \sum_{J'} \left[\frac{1}{2J''+1} S_{J'}(J'') \left| D_{k'J',\upsilon''J''} \right|^2 \right], \quad (2)$$

where $k'J'$ describe the continuum states of the final electronic state. Here, g is the degeneracy factor, which is given by

$$g = \frac{2 - \delta_{0,\Lambda'+\Lambda''}}{2 - \delta_{0,\Lambda''}} \quad (3)$$

where Λ' and Λ'' are the electronic orbital angular momentum projected on the internuclear axis for the final and initial electronic states, respectively. $S_{J'}(J'')$ represents the Hönl–London factor, which is indicated as the dependence of spectral line intensities on the rotational quantum numbers and varies with electronic transitions and rotational branches. There are three single branches (P, Q, R) for singlet transitions. For a $^1\Sigma \rightarrow {}^1\Sigma$ transition, $S_{J'}(J'')$ can be expressed as

$$S_{J'}\left(J''\right) = \begin{cases} J'', & J' = J'' - 1 \quad \text{(P branch)} \\ J'' + 1, & J' = J'' + 1 \quad \text{(R branch)} \end{cases}. \quad (4)$$

For a $^1\Sigma \rightarrow {}^1\Pi$ transition, $S_{J'}(J'')$ can be described by

$$S_{J'}\left(J''\right) = \begin{cases} \left(J''-1\right)/2, & J' = J'' - 1 \quad \text{(P branch)} \\ \left(2J''+1\right)/2, & J' = J'' \quad \text{(Q branch)} \\ \left(J''+2\right)/2, & J' = J'' + 1 \quad \text{(R branch)} \end{cases}. \quad (5)$$

Here, $D^{fi}_{k'J',\upsilon''J''}$ is the matrix element of the electric dipole transition moment for absorption from the rovibrational levels $\upsilon''J''$ in state i to the continuum $k'J'$ in state f. It is given by

$$D^{fi}_{k'J',\upsilon''J''} = \left\langle \chi_{k'J'}(R) \left| D^{fi}(R) \right| \chi_{\upsilon''J''}(R) \right\rangle, \quad (6)$$

where $\chi_{k'J'}(R)$ is the continuum wavefunction of the final electronic state f, $\chi_{\upsilon''J''}(R)$ is the bound rovibrational wavefunction of the initial electronic state i and $D_{fi}(R)$ is the TDM for an electronic transition. The bound and continuum rovibrational wavefunctions were solved by the renormalized Numerov method (Johnson 1977, 1978).

Assuming a Boltzmann population distribution for the rovibrational levels in the electronic ground state, the LTE cross section for photodissociation as a function of both temperature T and wavelength λ is given by

$$\sigma(\lambda, T) = \sum_{\upsilon''J''} \frac{\left(2J''+1\right) \exp\left(-\left|E_{\upsilon''J''} - E_{00}\right|/k_{\rm b}T\right) \sigma_{\upsilon''J''}}{Q(T)}. \quad (7)$$

Here, $E_{\upsilon''J''}$ is the rovibrational level $\upsilon''J''$, $k_{\rm b}$ is the Boltzmann constant and Q (T) is the partition function, given by

$$Q(T) = \sum_{\upsilon''J''} \left(2J''+1\right) \exp\left(-\left|E_{\upsilon''J''} - E_{00}\right|/k_{\rm b}T\right). \quad (8)$$

Based on the calculated photodissociation cross sections, the photodissociation rate for a molecule due to absorption of a photon in an ultraviolet radiation field can be calculated by

$$k = \int \sigma(\lambda) I(\lambda) \, {\rm d}\lambda, \quad (9)$$

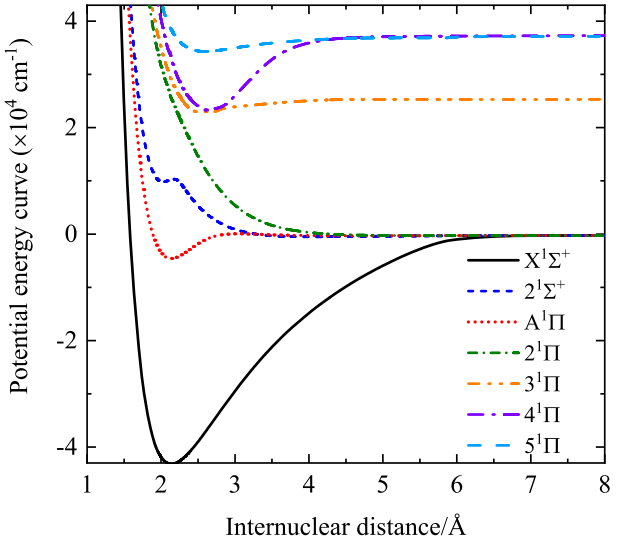

Figure 1. The PECs of the $X^1\Sigma^+$, $2^1\Sigma^+$, $A^1\Pi$, $2^1\Pi$, $3^1\Pi$, $4^1\Pi$ and $5^1\Pi$ states of AlCl along the internuclear distance. These curves are calculated at the icMRCI + Q/AV6Z level of theory.

where $\sigma(\lambda)$ is the photodissociation cross section and $I(\lambda)$ is the photon intensity of the radiation field. For a blackbody radiation field, the intensity is expressed as a function of temperature T and wavelength λ

$$I(\lambda, T) = \frac{8\pi c/\lambda^4}{\exp(hc/k_b T\lambda) - 1}, \quad (10)$$

where h is the Planck constant and c is the speed of light in vacuum. For the ISRF, the average intensity is estimated from the number and distribution of hot stars in the Galaxy, as well as a model for the dust distribution and its extinction of the stellar radiation (Habing 1968; Draine 1978; Mathis et al. 1983; Parravano et al. 2003; Heays et al. 2017). The ISRF intensity was fitted to an analytical expression by Draine (1978) for wavelengths within the range 91.2–200 nm:

$$I(\lambda) = 3.2028 \times 10^{13}\lambda^{-3} - 5.1542 \times 10^{15}\lambda^{-4} + 2.0546 \times 10^{17}\lambda^{-5}. \quad (11)$$

This expression was extended to 2000 nm by van Dishoeck & Black (1982)

$$I(\lambda) = 3.67 \times 10^{4}\lambda^{0.7}. \quad (12)$$

3. RESULTS AND DISCUSSION

3.1 PECs and TDMs

The computed PECs of seven singlet electronic states ($X^1\Sigma^+$, $2^1\Sigma^+$, $A^1\Pi$, $2^1\Pi$, $3^1\Pi$, $4^1\Pi$ and $5^1\Pi$) are displayed in Fig. 1 along the internuclear distance R. These curves are given in cm^{-1} relative to the first dissociation limit Al ($3s^2\ 3p\ ^2P$) + Cl ($3s^2 3p^5\ ^2P$). The $X^1\Sigma^+$, $2^1\Sigma^+$, $A^1\Pi$ and $2^1\Pi$ states converge into the Al ($3s^2 3p\ ^2P$) + Cl ($3s^2 3p^5\ ^2P$) asymptote. The $3^1\Pi$ state dissociates to the Al ($3s^2 4s\ ^2S$) + Cl ($3s^2 3p^5\ ^2P$) asymptote and the $4^1\Pi$ state correlates to the Al ($3s^2 3d\ ^2D$) + Cl ($3s^2 3p^5\ ^2P$) dissociation limit. In our calculations, the $2^1\Pi$ state is totally repulsive. As for the other six electronic states, the calculated spectroscopic constants are listed in Table 1 along with those of previous theoretical calculations and experiments where available.

The $X^1\Sigma^+$ state is deeply bound with an equilibrium internuclear distance R_e of 2.136 Å and an estimated dissociation energy D_e of 43 037 cm^{-1}. The calculated R_e is in good agreement with the experimental values of 2.130 11 Å observed by Wyse & Gordy (1972) and of 2.130 143 36 Å observed by Hedderich et al. (1993), as well as with the calculated values of 2.140 Å, 2.140 Å, 2.1374 Å and 2.1283 Å obtained by Langhoff et al. (1988), Brites et al. (2008), Wan et al. (2016) and Yousefi & Bernath (2018), respectively. Experimental estimates for the dissociation energy were given by Bhaduri & Fowler (1934) and Ram et al. (1982). Bhaduri & Fowler (1934) estimated a D_0 value of 5.16 ± 0.04 eV from thermochemical measurements. Ram et al. (1982) gave an upper limit for the D_0 value of 5.25 ± 0.01 eV from optical experiments. The D_0 values are converted to D_e values in cm^{-1} and are presented in Table 1. Good agreement can be observed between our results and the experimental results. Our result for D_e also agrees well with *ab initio* values of 42 752 cm^{-1} and 42 055 cm^{-1} computed by Langhoff et al. (1988) and Wan et al. (2016), respectively. Other spectroscopic constants of the $X^1\Sigma^+$ state, especially the harmonic frequency ω_e, are in excellent agreement with the experimental data and previous theoretical values.

The first singlet excited $A^1\Pi$ state is calculated to lie at 38 616 cm^{-1} with a weakly bound potential well of 4648 cm^{-1}. The relative error with the experiment (Huber & Herzberg 1979) for the T_e value is 362 cm^{-1} (0.93 %). The calculated R_e is 2.138 Å, which is 0.014 Å larger than the experimentally determined one of 2.124 Å. As for ω_e, our result is only 2.16 cm^{-1} smaller than the experimental value of 449.96 cm^{-1} (Huber & Herzberg 1979). The rotation constant B_e is predicted to be 0.242 93 cm^{-1}. The percentage error for the B_e value is 0.99 % relative to the experimental value (Huber & Herzberg 1979). No experimental data are available to compare D_e values. In addition, there is good agreement between the calculated spectroscopic constants and previous theoretical results for the $A^1\Pi$ state. For higher $2^1\Sigma^+$, $3^1\Pi$, $4^1\Pi$ and $5^1\Pi$ states, no experimental data are available for spectroscopic information. The $2^1\Sigma^+$ state has a shallow potential well above its dissociation limit and only supports one vibrational level. The minimum of the potential well is 52 945 cm^{-1} at R = 2.021 Å. The $3^1\Pi$ state has a calculated equilibrium internuclear distance of 2.510 Å also with a shallow potential well of 2435 cm^{-1}, but can carry 19 vibrational levels. The $4^1\Pi$ and $5^1\Pi$ states are calculated to locate at about 65 988 cm^{-1} and 77 133 cm^{-1}, respectively. Note that the energy difference between the dissociation limit of the $4^1\Pi$ and $5^1\Pi$ states and the first dissociation limit, Al ($3s^2 3p\ ^2P$) + Cl ($3s^2 3p^5\ ^2P$), is larger than that found in the NIST Atomic Spectra Database (Kramida et al. 2020). Hence, the PECs of the $4^1\Pi$ and $5^1\Pi$ states are shifted so as to match the separated atom energy difference in the NIST Atomic Spectra Database in the subsequent calculations of cross sections.

The TDMs of six transitions from the $2^1\Sigma^+$, $A^1\Pi$, $2^1\Pi$, $3^1\Pi$, $4^1\Pi$ and $5^1\Pi$ states to the ground $X^1\Sigma^+$ state for AlCl are calculated and displayed in Fig. 2. To verify our TDM calculations, we compared the TDM values of the $A^1\Pi$–$X^1\Sigma^+$ transition with the theoretical results calculated by Wan et al. (2016) in Fig. 3. As shown in Fig. 3, these two sets of TDM values show excellent agreement. Moreover, we determined the spontaneous radiative lifetime for the $A^1\Pi$–$X^1\Sigma^+$ system for comparison with available experimental and theoretical results (Rogowski & Fontijn 1987; Langhoff et al. 1988; Brites et al. 2008; Wan et al. 2016). The radiative lifetime τ ($\upsilon' = 0$) for the $A^1\Pi$ state is 5.67 ns, which is in good agreement with the experimental value of 6.4 ± 2.5 ns reported by Rogowski & Fontijn (1987) and previous *ab initio* results of 5.17, 5.9 and 4.99 ns calculated by Langhoff et al. (1988), Brites et al. (2008) and Wan et al. (2016), respectively.

Table 1. Spectroscopic constants of the $X^1\Sigma^+$, $A^1\Pi$, $2^1\Sigma^+$, $3^1\Pi$, $4^1\Pi$ and $5^1\Pi$ states of AlCl along with available experimental and theoretical values.

State	Source	R_e (Å)	T_e (cm^{-1})	ω_e (cm^{-1})	$\omega_e x_e$(cm^{-1})	B_e (cm^{-1})	D_e (cm^{-1})
$X^1\Sigma^+$	This work	2.136	0.00	484.9	2.269	0.241 63	43 037
	Calc.[a]	2.140	0.00	500			42 752
	Calc.[b]	2.140	0.00	484.5	6.47	0.2418	
	Calc.[c]	2.1374	0.00	478.13		0.2408	42 055
	Calc.[d]	2.1283	0.00	484.8065	2.069 68	0.244 1156	
	Expt.[e]	2.130 143 36	0.00	481.7765	2.101 81	0.243 900 66	42 584 ± 423[f]
$A^1\Pi$	This work	2.138	38 616	447.8	4.888	0.242 93	4648
	Calc.[a]	2.138	38 656	476			
	Calc.[b]	2.132	38 795	453.0	8.03	0.2435	
	Calc.[c]	2.1330	38 223.98	454.24		0.2397	4390
	Expt.[g]	2.124	38 254	449.96	4.37	0.245 375[f]	
$2^1\Sigma^+$[h]	This work	2.021	52 945				592
$3^1\Pi$	This work	2.510	65 898	486.0	57.53	0.178 95	2435
$4^1\Pi$	This work	2.672	65 988	483.9	13.81	0.154 99	14 567
$5^1\Pi$	This work	2.591	77 133	191.1	4.303	0.164 64	3104

[a] Langhoff et al. (1988). [b] Brites et al. (2008). [c] Wan et al. (2016). [d] Yousefi & Bernath (2018). [e] Hedderich et al. (1993). [f] Ram et al. (1982). [g] Huber & Herzberg (1979). [h] The $2^1\Sigma^+$ state can only support one vibrational level with the energy of 311.2264 cm^{-1} relative to its minimum value.

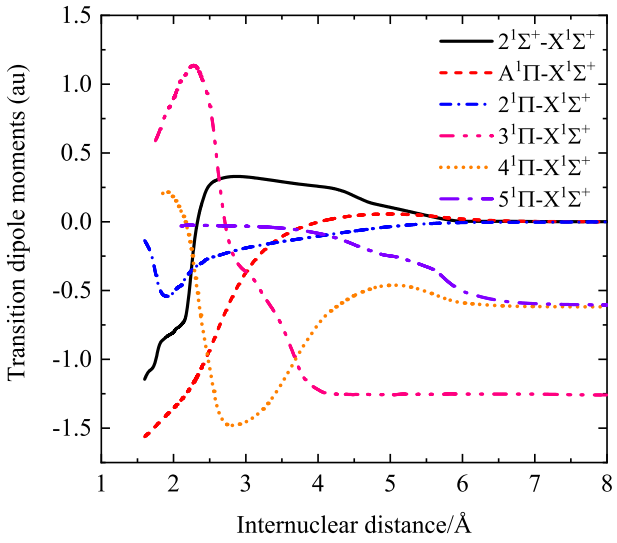

Figure 2. The TDMs for transitions from the $2^1\Sigma^+$, $A^1\Pi$, $2^1\Pi$, $3^1\Pi$, $4^1\Pi$ and $5^1\Pi$ states to the ground $X^1\Sigma^+$ state. These values are calculated at the icMRCI/AV6Z level of theory.

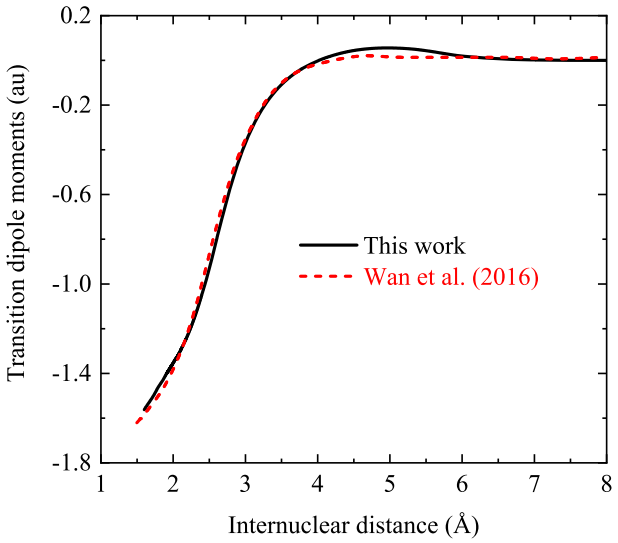

Figure 3. Comparison of the TDMs for the $A^1\Pi$–$X^1\Sigma^+$ transition with those calculated by Wan et al. (2016).

To compute the cross sections and rate coefficients, the PECs and TDMs are needed to extrapolate to the short and long ranges of the internuclear distance. For internuclear distances larger than 8 Å, the PECs and TDMs were extrapolated by the following function:

$$V(R) = -\frac{C_5}{R^5} - \frac{C_6}{R^6} + V(R \to \infty). \quad (13)$$

Here, C_6 is the dipole–dipole dispersion coefficient, which can be calculated by the London formula

$$C_6 = \frac{3}{2}\frac{\Gamma_{Al}\Gamma_{Cl}}{\Gamma_{Al}+\Gamma_{Cl}}\alpha_{Al}\alpha_{Cl}, \quad (14)$$

in which Γ_{Al} and Γ_{Cl} are the ionization energies of the atomic Al and Cl states, respectively, which can be obtained from the NIST Atomic Spectra Database (Kramida et al. 2020), and α is the dipole polarizability of an atomic state. The dipole polarizability of α_{Al} for the ground state Al ($3s^2\,3p\ ^2P$) is 57.8 (Schwerdtfeger & Nagle 2019). For the ground state $3s^2\,3p^5\,^2P$ of Cl, a dipole polarizability of $\alpha_{Cl} = 14.6$ is used (Schwerdtfeger & Nagle 2019). The α_{Al} of excited states Al ($3s^2\,4s\ ^2S$) and Al ($3s^2\,3d\ ^2D$) are estimated as the same value of the ground state Al ($3s^2\,3p\ ^2P$) here. C_5 is estimated by fitting *ab initio* points while keeping the dissociation limits and C_6 fixed. The obtained C_5 and C_6 are given in Table 2. The short-range PECs and TDMs down to an internuclear distance R of 0.5 Å were extrapolated by the following expression:

$$V(R) = A\exp(-BR) + C. \quad (15)$$

A cubic spline was applied to interpolate the *ab initio* points of PECs and TDMs.

3.2 State-resolved cross sections

Based on the theory given in Section 2.2, photodissociation cross sections of AlCl have been calculated for transitions from 38 958 initial rovibrational levels ($v'' \leq 100$, $J'' \leq 400$) in the ground $X\ ^1\Sigma^+$ state to five excited electronic states. Cross sections were computed

Table 2. Dissociation relationship of the $X^1\Sigma^+$, $A^1\Pi$, $2^1\Sigma^+$, $2^1\Pi$, $3^1\Pi$, $4^1\Pi$ and $5^1\Pi$ states for AlCl.

Molecular state	Dissociation limit			C_5[c]	C_6[c]
	Atomic state	Energy (cm^{-1})[a]	Energy (cm^{-1})[b]		
$X^1\Sigma^+$	Al ($3s^2$ $3p$ ^2P) + Cl ($3s^2$ $3p^5$ ^2P)	0.00	0.00	29.4	196.73
$A^1\Pi$	Al ($3s^2$ $3p$ ^2P) + Cl ($3s^2$ $3p^5$ ^2P)	0.00	0.00	26.0	196.73
$2^1\Sigma^+$	Al ($3s^2$ $3p$ ^2P) + Cl ($3s^2$ $3p^5$ ^2P)	0.00	0.00	7.38	196.73
$2^1\Pi$	Al ($3s^2$ $3p$ ^2P) + Cl ($3s^2$ $3p^5$ ^2P)	0.00	0.00	74.2	196.73
$3^1\Pi$	Al ($3s^2$ $4s$ ^2S) + Cl ($3s^2$ $3p^5$ ^2P)	25 347.756	25 318.42	0.00	89.66
$4^1\Pi$	Al ($3s^2$ $3d$ ^2D) + Cl ($3s^2$ $3p^5$ ^2P)	32 435.453	36 943.28	79.0	68.80
$5^1\Pi$	Al ($3s^2$ $3d$ ^2D) + Cl ($3s^2$ $3p^5$ ^2P)	32 435.453	36 642.75	89.9	68.80

[a] Experimental data from NIST Atomic Spectra Database (Kramida et al. 2020). [b] This work. [c] Estimated (see the text for details).

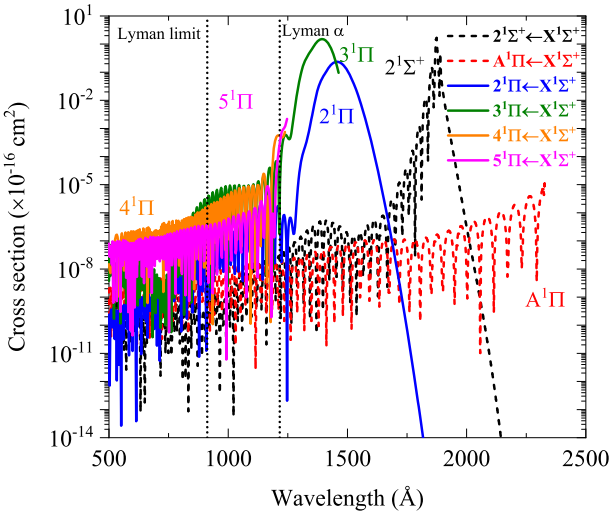

Figure 4. State-resolved cross sections of AlCl as a function of wavelengths for transitions from the rovibrational level $(\upsilon'', J'') = (0, 0)$ of the ground $X^1\Sigma^+$ state to the excited $2^1\Sigma^+$, $A^1\Pi$, $2^1\Pi$, $3^1\Pi$, $4^1\Pi$ and $5^1\Pi$ states.

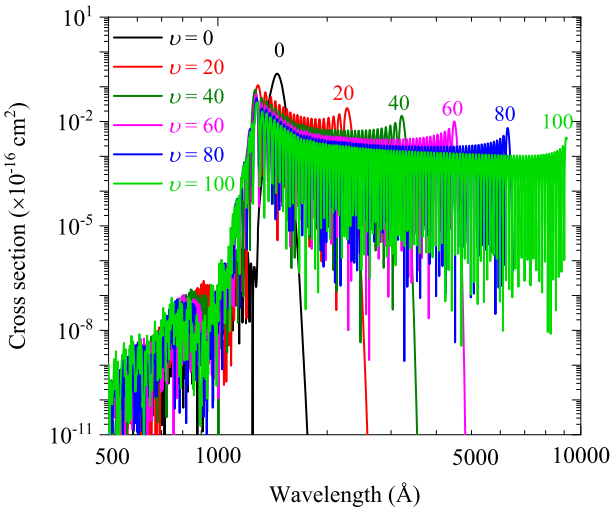

Figure 5. State-resolved cross sections of AlCl as a function of wavelengths for the $2^1\Pi$–$X^1\Sigma^+$ transition from several vibrational levels with the rotational quantum number $J'' = 0$.

as a function of photon wavelengths from 500 Å to the dissociation threshold. Fig. 4 shows a comparison of the state-resolved cross sections from rovibrational level (υ'', J'') = (0, 0) for the considered six transitions, including $2^1\Sigma^+ \leftarrow X^1\Sigma^+$, $A^1\Pi \leftarrow X^1\Sigma^+$, $2^1\Pi \leftarrow X^1\Sigma^+$, $3^1\Pi \leftarrow X^1\Sigma^+$, $4^1\Pi \leftarrow X^1\Sigma^+$ and $5^1\Pi \leftarrow X^1\Sigma^+$. The $2^1\Sigma^+ \leftarrow X^1\Sigma^+$, $2^1\Pi \leftarrow X^1\Sigma^+$ and $3^1\Pi \leftarrow X^1\Sigma^+$ transitions contribute significantly to the cross sections of AlCl, while the $A\ ^1\Pi \leftarrow X^1\Sigma^+$ transition makes little contribution. To exhibit the variation of the cross section with different vibrational and rotational quantum numbers, a selection of the state-resolved cross sections for the $2\ ^1\Pi \leftarrow X^1\Sigma^+$ transition as a function of photon wavelength is displayed in Fig. 5 for $J'' = 0$ and a set of selected υ'', and shown in Fig. 6 for $\upsilon'' = 0$ and a set of selected J''. As expected, the cross sections tend to larger photon wavelength due to the decreasing photon threshold energy with increasing υ'' and/or J''.

3.3 LTE cross sections

The temperature-dependent cross sections in LTE were computed for the considered six transitions mentioned above by equation (7) from 500 to 10 000 K, where a comparison of LTE cross sections at 500 K for each transition is displayed in Fig. 7. At wavelengths smaller than 1500 Å, the photodissociation processes through $3^1\Pi$, $4^1\Pi$ and $5^1\Pi$ states are dominant. As the wavelength increases, the photodissociation processes of the $2^1\Pi \leftarrow X^1\Sigma^+$, $2^1\Sigma^+ \leftarrow X^1\Sigma^+$

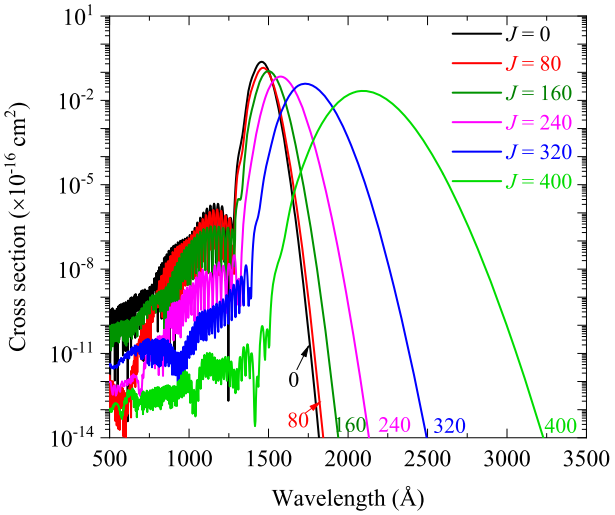

Figure 6. State-resolved cross sections of AlCl as a function of wavelengths for the $2^1\Pi$–$X^1\Sigma^+$ transition from the vibrational level $\upsilon'' = 0$ with several rotational quantum numbers.

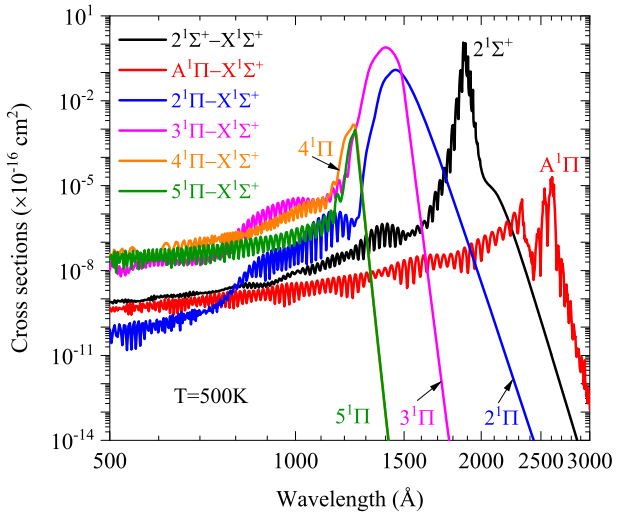

Figure 7. Temperature-dependent cross sections of AlCl in LTE for transitions from the ground state to the excited $2^1\Sigma^+$, $A^1\Pi$, $2^1\Pi$, $3^1\Pi$, $4^1\Pi$ and $5^1\Pi$ states at 1000 K.

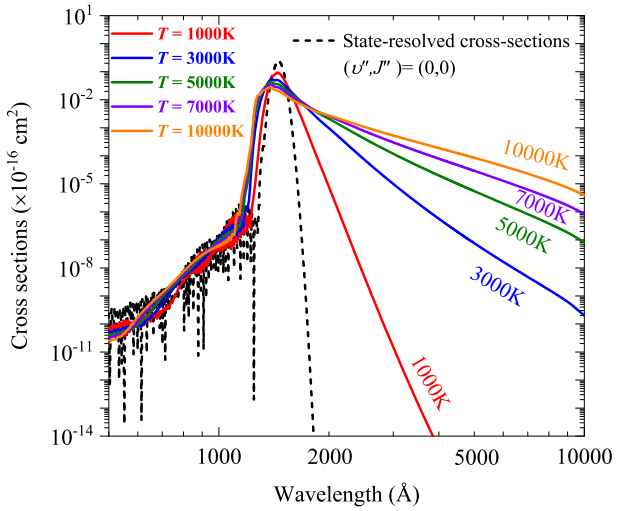

Figure 8. Temperature-dependent cross sections of AlCl in LTE for the $2^1\Pi \leftarrow X^1\Sigma^+$ transition at several kinetic temperatures. The $(\upsilon'', J'') = (0, 0)$ state-resolved cross section is included for comparison.

and $A^1\Pi \leftarrow X^1\Sigma^+$ transitions play an important role consecutively. A sample of LTE cross sections for the $2\,^1\Pi \leftarrow X^1\Sigma^+$ transition at several kinetic temperatures is shown in Fig. 8. As shown, the peaks of the cross sections drop gradually as the temperature increases. At wavelengths larger than about 2000 Å, the cross sections increase when the temperature increases.

3.4 Photodissociation rates

Fig. 9 shows the calculated temperature-dependent photodissociation rates of AlCl in LTE for all six electronic transitions in the blackbody radiation field, when the temperature of gas was assumed to be the same as the radiation temperature. As shown in Fig. 9, the photodissociation rate increases as the temperature of gas increases for all the electronic transitions considered here. Moreover, the photodissociation rates in the ISRF were investigated (Draine 1978; Heays et al. 2017). In general, the gas temperature is not expected

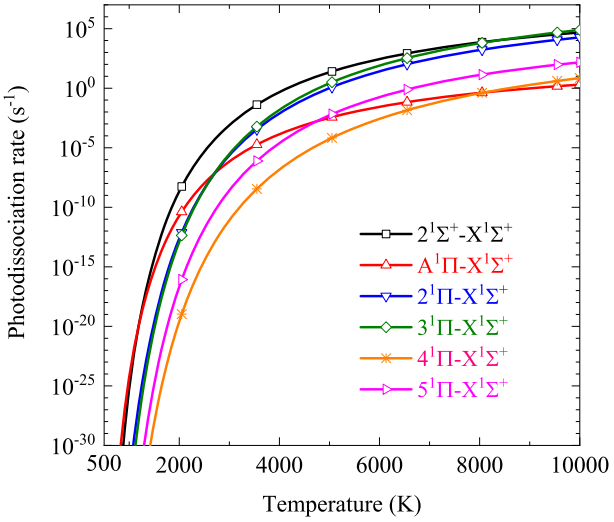

Figure 9. Temperature-dependent photodissociation rates of AlCl in LTE for each electronic transition in the blackbody radiation field when kinetic and radiation temperatures are equal.

to be above 100 K in the ISRF. Hence, the rates were calculated based on the state-resolved cross sections (υ'', J'') = (0, 0) and LTE cross sections below 100 K for the six electronic transitions (see Table 3). The results show the significant importance for the $3^1\Pi \leftarrow X^1\Sigma^+$ transition, which provides about 76 % contribution of the total photodissociation rate.

The highest electronic state in this work is considered to be the $4^1\Pi$ state, which dissociates into the Al ($3s^2\,3d\ ^2$D) + Cl ($3s^2\,3p^5\,^2$P) asymptote. Higher electronic states correlating to the higher dissociation limits between the Al ($3s^2\,3d\ \ ^2$D) + Cl ($3s^2\,3p^5\,^2$P) and Al^+ ($3s^2\,^1$S$_0$) + Cl ($3s^2\,3p^5\,^2$P) asymptotes may contribute to the cross sections below 3087 Å. Especially, the thresholds of the cross sections for transitions from these higher electronic states to the ground state may provide a significant contribution to the interstellar radiation for wavelengths from 1102 to 1335 Å. Hence, the photodissociation rates calculated here are lower limits.

4. CONCLUSION

At the icMRCI + Q/AV6Z level of theory, PECs and TDMs of AlCl have been constructed and used to perform comprehensive calculations for the photodissociation cross sections of AlCl through $2^1\Sigma^+ \leftarrow X^1\Sigma^+$, $A^1\Pi \leftarrow X^1\Sigma^+$, $2^1\Pi \leftarrow X^1\Sigma^+$, $3^1\Pi \leftarrow X^1\Sigma^+$, $4^1\Pi \leftarrow X^1\Sigma^+$ and $5^1\Pi \leftarrow X^1\Sigma^+$ transitions. The state-resolved and temperature-dependent LTE cross sections of these six transitions have also been evaluated for a total of 38 958 rovibrational levels ($\upsilon'' \leq 100$, $J'' \leq 400$) of the ground state $X^1\Sigma^+$ for AlCl and over a large range of wavelengths. The results of LTE cross sections have then been used to compute photodissociation rates of AlCl in the interstellar and blackbody radiation fields. It is hoped that the photodissociation cross sections and rates obtained in this work will be useful for investigating the abundance of AlCl in envelopes around evolved stars, such as carbon-rich and oxygen-rich stars.

ACKNOWLEDGEMENTS

This work is sponsored by the National Natural Science Foundation of China (51421063, 52106098). Zhi Qin also acknowledges the support from Postdoctoral Innovation Project of Shandong Province

Table 3. Photodissociation rates (s^{-1}) of AlCl under the standard ISRF.

Transition	State-resolved cross section (υ'', J'') = (0, 0)	LTE cross section		
		10K	50K	100K
$2^1\Sigma^+ \leftarrow X^1\Sigma^+$	2.68×10^{-10}	2.67×10^{-10}	2.68×10^{-10}	2.69×10^{-10}
$A^1\Pi \leftarrow X^1\Sigma^+$	7.13×10^{-15}	5.12×10^{-15}	4.15×10^{-15}	3.61×10^{-15}
$2^1\Pi \leftarrow X^1\Sigma^+$	4.41×10^{-10}	2.99×10^{-10}	2.95×10^{-10}	2.94×10^{-10}
$3^1\Pi \leftarrow X^1\Sigma^+$	2.53×10^{-09}	1.71×10^{-09}	1.69×10^{-09}	1.69×10^{-09}
$4^1\Pi \leftarrow X^1\Sigma^+$	5.52×10^{-13}	3.71×10^{-13}	3.55×10^{-13}	3.48×10^{-13}
$5^1\Pi \leftarrow X^1\Sigma^+$	8.79×10^{-12}	5.92×10^{-12}	5.78×10^{-12}	5.74×10^{-12}
All $^1\Pi \leftarrow X^1\Sigma^+$	3.06×10^{-09}	2.02×10^{-09}	1.99×10^{-09}	1.99×10^{-09}
Total	3.33×10^{-09}	2.29×10^{-09}	2.26×10^{-09}	2.26×10^{-09}

and Postdoctoral Applied Research Project of Qingdao. The scientific calculations in this paper have been done on the HPC Cloud Platform of Shandong University.

DATA AVAILABILITY STATEMENT

Full data are available. The cross sections and rate coefficients can be obtained online at https://dr-zhi-qin.github.io/personal/Database.html . The supplemental materials include the calculated PECs and TDMs for AlCl (corresponding to Figs 1 and 2), the MOLPRO input file and the LTE photodissociation rates in the blackbody radiation field (corresponding to Fig. 9).

REFERENCES

Agúndez M., Fonfría J., Cernicharo J., Kahane C., Daniel F., Guélin M., 2012, A&A, 543, A48
Asplund M., Grevesse N., Sauval A.J., Scott P., 2009, ARA&A, 47, 481
Babb J.F., 2015, ApJS, 216, 21
Bai T., Qin Z., Liu L., 2021, MNRAS, 505, 2177
Bates D.R., Spitzer L., Jr, 1951, ApJ, 113, 441
Benna M., Mahaffy P., Grebowsky J., Plane J., Yelle R., Jakosky B., 2015, Geophys. Res. Lett., 42, 4670
Bhaduri B., Fowler A., 1934, Proc. R. Soc. Lond A, 145, 321
Bieler A. et al., 2015, Nature, 526, 678
Black J.H., 1989, in: Bates D., Bederson B. eds., Advances in Atomic and Molecular Physics. Academic, New York, p. 477
Brites V., Hammoutene D., Hochlaf M., 2008, J. Phys. Chem. A, 112, 13419
Cernicharo J., Guelin M., 1987, A&A, 183, L10
Crovisier J., Leech K., Bockelee-Morvan D., Brooke T. Y., Hanner M. S., Altieri B., Keller H. U., Lellouch E., 1997, Science, 275, 1904
Decin L. et al., 2017, A&A, 608, A55
Draine B.T., 1978, ApJS, 36, 595
Eddington A. S., 1928, MNRAS, 88, 352
El-Qadi W., Stancil P., 2013, ApJ, 779, 97
Grebenshchikov S.Y., 2016, J. CO2 Utilization, 15, 32
Habing H., 1968, Bull. Astr. Inst. Netherlands, 19, 421
Heays A., Bosman A., Van Dishoeck E., 2017, A&A, 602, A105
Hedderich H.G., Dulick M., Bernath P.F., 1993, J. Chem. Phys., 99, 8363
Huber K.-P., Herzberg G., 1979, Molecular Spectra and Molecular Structure: IV. Constants of Diatomic Molecules.Van Nostrand Reinhold, New York
Johnson B. R., 1977, J. Chem. Phys., 67, 4086
Johnson B. R., 1978, J. Chem. Phys., 69, 4678
Kirby K. P., Van Dishoeck E. F., 1989, in: Bates D., Bederson B. eds., Advances in Atomic Molecular Physics. Academic Press, New York, p. 437
Knowles P. J., Werner H.-J., 1985, Chem. Phys. Lett., 115, 259
Knowles P. J., Werner H.-J., 1988, Chem. Phys. Lett., 145, 514
Knowles P. J., Werner H.-J., 1992, Theor. Chim. Acta, 84, 95
Kramers H. A., Ter Haar D., 1946, Bull. Astr. Inst. Netherlands, 10, 137
Kramida A., Ralchenko Y., Reader J., NIST ASD Team, 2020, NIST Atomic Spectra Database (version 5.8), https://physics.nist.gov/asd
Langhoff S. R., Bauschlicher C. W., Taylor P. R., 1988, J. Chem. Phys., 88, 5715
Larsson M., Geppert W., Nyman G., 2012, Rep. Prog. Phys., 75, 066901
Lodders K., Fegley B., 2006, in Mason J. W., ed., Astrophysics Update 2. Praxis Publishing, Chichester, p. 1
Loreau J., Lecointre J., Urbain X., Vaeck N., 2011, Phys. Rev. A, 84, 053412
Mathis J., Mezger P., Panagia N., 1983, A&A, 128, 212
McMillan E., Shen G., McCann J., McLaughlin B., Stancil P., 2016, J. Phys. B, 49, 084001
Miyake S., Gay C., Stancil P., 2011, ApJ, 735, 21
Parravano A., Hollenbach D.J., McKee C.F., 2003, ApJ, 584, 797
Pattillo R. J., Cieszewski R., Stancil P. C., Forrey R. C., Babb J. F., McCann J. F., McLaughlin B. M., 2018, ApJ, 858, 10
Pezzella M., Yurchenko S. N., Tennyson J., 2021, Phys. Chem. Chem. Phys., 23, 16390
Qin Z., Bai T., Liu L., 2021, ApJ, 917, 87
Ram R. S., Rai S. B., Upadhya K. N., Rai D. K., 1982, Phys. Scr., 26, 383
Rogowski D. F., Fontijn A., 1987, Chem. Phys. Lett., 137, 219
Schwerdtfeger P., Nagle J. K., 2019, Mol. Phys., 117, 1200
Shamasundar K., Knizia G., Werner H.-J., 2011, J. Chem. Phys., 135, 054101
Snow T. P., Bierbaum V. M., 2008, Annu. Rev. Anal. Chem., 1, 229
Valiev R., Berezhnoy A., Gritsenko I., Merzlikin B., Cherepanov V. N., Kurten T., Wöhler C., 2020, A&A, 633, A39
van Dishoeck E. F., 1998, The Chemistry of Diffuse and Dark Interstellar Clouds. Oxford University Press, Oxford
van Dishoeck E. F., Black J., 1982, ApJ, 258, 533
van Dishoeck E. F., Blake G. A., 1998, ARA&A, 36, 317
Visser R., Van Dishoeck E., Black J. H., 2009, A&A, 503, 323
Wan M., Yuan D., Jin C., Wang F., Yang Y., Yu Y., Shao J., 2016, J. Chem. Phys., 145, 341
Weck P., Stancil P., Kirby K., 2003, ApJ, 582, 1263
Werner H.-J. et al., 2020, J. Chem. Phys., 152, 144107
Werner H. J., Knowles P. J., 1985, J. Chem. Phys., 82, 5053
Werner H. J., Knowles P. J., 1988, J. Chem. Phys., 89, 5803
Werner H. J. et al., 2015, MOLPRO 2015, a package of ab initio programs, see http://www.molpro.net
Wyse F., Gordy W., 1972, J. Chem. Phys., 56, 2130
Xu Z., Luo N., Federman S., Jackson W. M., Ng C-Y., Wang L-P., Crabtree K. N., 2019, ApJ, 882, 86
Yang Y. K., Cheng Y., Peng Y. G., Wu Y., Wang J. G., Qu Y. Z., Zhang S. B., 2020, J. Quant. Spectrosc. Radiat. Transfer, 254, 107203
Yousefi M., Bernath P. F., 2018, ApJS, 237, 8
Zammit M. C. et al., 2017, ApJ, 851, 64

SUPPORTING INFORMATION

Supplementary data are available at *MNRAS* online.

Supplemental material.zip

Please note: Oxford University Press is not responsible for the content or functionality of any supporting materials supplied by the authors. Any queries (other than missing material) should be directed to the corresponding author for the article.

This paper has been typeset from a TEX/LATEX file prepared by the author.